Analytica Chimica Acta 1384 (2026) 344964

Contents lists available at ScienceDirect

Analytica Chimica Acta

journal homepage: www.elsevier.com/locate/aca

Aptamer conformation sensing in nanopore for on-site quantitative detection of cadmium ions at nanomolar concentrations

Shujun He [a,1], Ronghui Liu [b,*,1], Xinxin Bao [c,1], Jiayuan Pang [b], Xi Zhang [b], Yue Liu [b], Wenfu Lin [b], Jiadun Liu [b], Tianxin Li [a], Yao Li [c,**], Yi Li [b,***], Xinrong Guo [a,d,****]

[a] The First Dongguan Affiliated Hospital, Guangdong Medical University, Dongguan, 523808, China
[b] School of Microelectronics, Southern University of Science and Technology, Shenzhen, 518055, China
[c] School of Physics and Key Laboratory of Functional Polymer Materials of Ministry of Education, Nankai University, Collaborative Innovation Center of Chemical Science and Engineering, Tianjin, 300071, China
[d] School of Public Health, Guangdong Medical University, Dongguan, 523808, China

HIGHLIGHTS

- Aptamer-enhanced nanopore sensing enables selective Cd^{2+} detection.
- A low limit of detection (33.80 nM) can be achieved, meeting stringent water quality standards.
- This method demonstrates broad applicability across diverse water matrices, from freshwater to seawater.

GRAPHICAL ABSTRACT

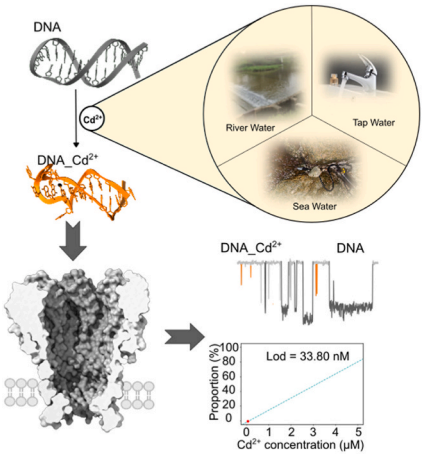

ARTICLE INFO

Handling Editor: Dr. J.P. Landers

Keywords:
Nanopore sensing
Cd^{2+} detection

ABSTRACT

Background: The detection of heavy metal ions has traditionally relied on laboratory-based spectroscopy techniques, which are often time-consuming, complex, and unsuitable for real-time monitoring. To address this challenge, we introduce an aptamer conformation sensing strategy and evaluate its ability to detect cadmium ions. The sensing strategy qualitatively infers the isolation of cadmium ions (Cd^{2+}) by monitoring the docking

* Corresponding author.
** Corresponding author.
*** Corresponding author.
**** Corresponding author. The First Dongguan Affiliated Hospital, Guangdong Medical University, Dongguan, 523808, China.
E-mail addresses: liurh@sustech.edu.cn (R. Liu), liyao@nankai.edu.cn (Y. Li), liy37@sustech.edu.cn (Y. Li), guoxinr@gdmu.edu.cn (X. Guo).
[1] These authors contributed equally.

https://doi.org/10.1016/j.aca.2025.344964
Received 3 September 2025; Received in revised form 12 November 2025; Accepted 29 November 2025
Available online 1 December 2025

Aptamer conformation sensing
Molecular dynamics simulations

changes of a single DNA aptamer before and after binding with Cd^{2+} in the nanopore, and quantitatively determines the concentration by extracting the event count of characteristic events.
Result: Molecular dynamics simulations reveal that Cd^{2+} binding induces structural reconfiguration, reducing aptamer penetration depth from 5.20 nm (free DNA) to 1.66 nm (DNA_Cd^{2+}). Electrical signatures indicate that unbound aptamers produce sustained current blockades ($\Delta I/I_0 = 42$ %), while Cd^{2+} complexes generate transient signals ($\Delta I/I_0 = 25$ %). Dual-parameter analysis ($\Delta I/I_0$ vs. I_{rms}) provides precise detection. The sensor achieves a detection limit of 33.8 nM within 10 min and demonstrates >93-fold selectivity over Mn^{2+}, Ca^{2+}, Cu^{2+}, Co^{2+}, Ni^{2+}, and Fe^{3+}. Field validation shows detection accuracy consistent with ICP-MS results. *Significance*: These findings highlight the potential of nanopore-based aptamer conformation sensing as a powerful platform for real-time, quantitative detection of heavy metal ions in complex environmental matrices.

1. Introduction

Point-of-care detection of small molecules, particularly heavy metal ions, is critical in various fields, including environmental monitoring, food safety, and clinical diagnostics [1,2]. Traditional methods such as atomic absorption spectroscopy (AAS) and inductively coupled plasma mass spectrometry (ICP-MS) are highly effective but require expensive equipment [3–6], skilled personnel, and centralized laboratories, limiting their applicability in field settings [2,7]. Recent advances in nanopore sensing have introduced a promising alternative [8,9]. This method measures current fluctuations as ions or molecules translocate through nanoscale pores, enabling unprecedented sensitivity in detecting low-concentration analytes [9–11].

Nanopore-based sensors, such as α-hemolysin and MspA, have shown substantial potential for the selective detection of metal ions [12–14]. For example, α-HL modified with histidine residues selectively detects Zn^{2+} [15], while the M2-MspA-H variant discriminates multiple metal ions including Co^{2+}, Ni^{2+}, Zn^{2+}, and Pb^{2+} [16]. Recent innovations have further improved nanopore sensitivity by integrating synthetic ligands, such as Nα,Nα-bis(carboxymethyl)-L-lysine hydrate (ANTA) into the M2-MspA nanopore, to selectively capture and identify rare earth elements [17]. Despite these advances, quantitative detection of heavy metal ions remains challenging. Recognition elements often exhibit cross-reactivity, high concentrations are required to generate distinguishable signals, and complex sample matrices introduce interference that compromises reproducibility and accuracy.

Aptamers provide a compelling solution. These short, single-stranded nucleic acids offer high binding affinity, structural adaptability, and superior stability compared with antibodies [18–21]. Importantly, target binding induces distinct conformational changes that can be captured by nanopore readouts, offering a direct route to selective and quantitative detection [22–24]. Recent studies have shown that nanopores can resolve aptamer conformational dynamics in response to target binding [25,26], and can detect charge changes upon metal coordination [14], underscoring their potential for quantitative biosensing. However, whether such strategies can be extended to the selective and quantitative detection of toxic heavy metal ions, particularly Cd^{2+} in complex environmental matrices, remains unresolved.

In this study, we developed a nanopore-based sensing strategy that employs DNA aptamer conformational changes within engineered M2-MspA nanopores for the quantitative detection of Cd^{2+}. Ionic current measurements were used to monitor structural changes of the aptamer upon Cd^{2+} binding, and molecular dynamics simulations provided further insights into the aptamer–nanopore interaction. The influence of competing metal ions was systematically evaluated, and a quantitative detection model was established. The method achieved sensitive Cd^{2+} detection at nanomolar levels and was successfully applied to real water samples, demonstrating its potential for practical environmental analysis.

2. Experimental section

2.1. Materials and reagents

The DNA aptamer and the DNA encoding the M2-MspA variant sequence used in this study were synthesized by Qingke Biotechnology Co., Ltd. (Beijing, China). Random DNA was obtained from the DL1000 DNA Marker (Takara Bio, Inc., Japan). $CdCl_2$ and HCl were purchased from Aladdin Biochemical Technology Co., Ltd. (Shanghai, China), while $CaCl_2$, $FeCl_3$, $MnCl_2$, $CuCl_2$, $CoCl_2$, and $NiCl_2$, were obtained from Macklin, Meryer, and Energy Chemical Co., Ltd. All DNA and chemicals were dissolved in double-distilled water (ddH_2O). The buffer for nanopore experiment consisted of 1 M NaCl and 20 mM HEPES, adjusted to pH 7.3 with HCl.

2.2. Preparation of M2-MspA protein

The DNA sequence encoding the M2-MspA variant [27], with a C-terminal polyhistidine tag, was cloned into the pET-30a plasmid and expressed in *E. coli* BL21(DE3) cells. Cultures were grown to an OD_{600} of 0.8 and induced with 0.5 mM IPTG at 18 °C for 18 h. Cells were harvested by centrifugation at 6000 rpm, resuspended in lysis buffer (150 mM NaCl, 100 mM NaH_2PO_4, 100 mM Na_2HPO_4, 0.1 mM EDTA, 0.33 mM PMSF, 33.3 mM $MgCl_2$, 0.1 mg/mL DNase, pH 6.5), and lysed by ultrasonication. The lysate was treated with 0.5 % Genapol X-080 and mixed at 4 °C for 30 min, heated at 60 °C for 10 min, cooled to 4 °C, and centrifuged at 11,000×*g* for 10 min. The supernatant was applied to a nickel affinity column, washed with buffer 1 (500 mM NaCl, 20 mM HEPES, 0.5 % Genapol X-080, 5 mM imidazole, pH 8.0; 20 column volumes) and buffer 2 (500 mM NaCl, 20 mM HEPES, 0.5 % Genapol X-080, 40 mM imidazole, pH 8.0; 10 column volumes). The protein was eluted with elution buffer (500 mM NaCl, 20 mM HEPES, 0.5 % Genapol X-080, 500 mM imidazole, pH 8.0) and concentrated using a 30 kDa MWCO filter (Millipore). The M2-MspA octamer was then characterized by 12 % SDS-PAGE and directly used for electrophysiological measurements.

2.3. Circular dichroism (CD) spectroscopy test

CD experiments were conducted at room temperature using a CD spectrometer (Applied Photophysics Chirascan). Samples for CD tests were prepared in three distinct buffer systems: buffer A (1 M NaCl and 20 mM HEPES at pH 7.3), buffer B (1 M KCl, 20 mM HEPES, pH 7.3), and buffer C (20 mM Tris-HAc, 140 mM NaCl, 5 mM KCl, 10 mM $MgCl_2$, pH 7.4). Each sample was prepared by heating a mixture of DNA (10 μM) and Cd^{2+} ions (100 μM) at 95 °C for 5 min, followed by gradual cooling to room temperature.

Spectra were recorded for DNA samples in the absence and presence of Cd^{2+} over the wavelength range of 200–350 nm using a 1-mm quartz cuvette (Hellma Analytics). For each condition, three scans were collected with a bandwidth of 10 mm and a digital integration time of 0.5 s per point. All spectra were baseline-corrected using the corresponding buffer blanks. Data were analyzed and plotted using Origin software.

2.4. Nanopore experiment

The preparation of DNA and DNA_Cd^{2+} followed the protocols described above. Briefly, DNA was mixed with metal ions, heated at 95 °C for 5 min, and cooled to 4 °C. For real-world water samples (tap water, river water, and seawater), samples were allowed to settle for 3 h, filtered through a 0.22 μm membrane to remove impurities, spiked with Cd^{2+} at defined concentrations, and subjected to the same DNA incubation procedure.

Nanopore experiments were performed using a lipid bilayer composed of DPhPC formed on the MECA (Micro Electrode Cavity Array) recording substrate. The MECA chip consist of a 2 × 2 array of circular microcavities (100 μm) embedded in an inert polymer. M2-MspA protein was added to the bilayer until single nanopore insertion was confirmed by open-current monitoring. DNA or DNA_Cd^{2+} samples were then introduced, and current recordings were acquired at +100 mV. Each condition was examined in triplicate. Single-pore current recordings were performed using the Orbit mini system with a built-in four-channel amplifier. Data were acquired with Element Data Reader 3.8.18 at a sampling rate of 10 kHz and a maximum current range of 20 nA. All recordings were processed using a custom-modified version of Python [27].

2.5. Quantification of DNA specificity toward different metal ions

DNA specificity toward different metal ions was quantified based on event distributions within defined blockage ratio ranges. All experiments were conducted with a fixed DNA concentration of 4 μM and a metal ion concentration of 5 μM. Two complementary strategies were employed: a direct method (Method 1), which quantifies specific DNA_metal binding events occurring in the low blockage ratio region (12.5–30 %); and an indirect method (Method 2), which measures the reduction of typical DNA_only events in the 30–55 % range.

Method 1:

$$\text{Specificity}\ (\%) = \left(\frac{m_{x=12.5-30\%}}{m_0} - \frac{n_{x=12.5-30\%}}{n_0}\right) \times 100\%$$

where m_0 and n_0 are the total number of events in DNA_metal and DNA_only experiments, respectively, and $m_{x=12.5-30\%}$ and $n_{x=12.5-30\%}$ are the number of events in the 12.5–30 % range. This range was defined as the "signature region" for DNA_metal complex events, with the 30–35 % segment excluded to minimize overlap with unbound DNA. Background contributions from DNA_only events were subtracted to ensure accuracy.

Method 2:

$$\text{Specificity}\ (\%) = \left(\frac{n_{x=30-55\%}}{n_0} - \frac{m_{x=30-55\%}}{m_0}\right) \times 100\%$$

where m_0 and n_0 are the total numbers of events in DNA_metal and DNA_only experiments. where $n_{x=30-55\%}$ and $m_{x=30-55\%}$ represent the number of events in the 30–55 % range.

2.6. Establishment of a standard curve

To establish a quantitative relationship between Cd^{2+} concentration and nanopore signal response, 4 μM DNA was mixed with a series of graded concentrations of Cd^{2+}. Event distributions were analyzed based on their blockage ratios, which reflect changes in DNA conformation or translocation behavior induced by Cd^{2+} binding. Quantification was performed using two complementary calculation methods described above.

2.7. MD simulation

All molecular dynamics simulations were conducted using the GROMACS 2022 software package [28]with the CHARMM36 force field CHARMM-GUI web server [29]. Structures of the M2-MspA nanopore, DNA aptamer and Cd^{2+} binding aptamer were obtained from the Protein Data Bank (PDB) entries 1UUN and 8GZJ, respectively. A 12 × 12 nm^2 1, 2-Dioleoyl-*sn*-glycero-3-phosphocholine (DOPC) lipid bilayer was added to the system. The TIP3P water model [30] was used to fill the periodic rectangular simulation box, and Na^+ and Cl^- ions were added at random positions to achieve a salt concentration of 1.0 M and neutralize the system. The final systems contained approximately 310,000 atoms. Long-range electrostatic interactions beyond 1.2 Å-spaced grid were calculated using the particle mesh Ewald (PME) method [31], while the cutoff radius for van der Waals interactions was set to 1.2 nm. The V-rescale [31] thermostat maintained the temperature at 298.15 K, and the C-rescale [32] semi-isotropic barostat adjusted the system volume to maintain a pressure of 1 atm. The LINCS algorithm [33] was applied to constrain bonds containing hydrogen atoms, and the SETTLE algorithm [34] maintained the rigidity of water molecules. All simulations were performed with a 2 fs time step.

Following assembly, each system underwent energy minimization for approximately 4500 steps to ensure that the maximum force was less than 1000 kJ/mol/nm^2. Subsequently, a 10 ns equilibration was performed under the constant number of atoms, pressure, and temperature (NPT) ensemble. During the equilibration phase, harmonic positional restraints with a spring constant of 500 kJ/mol/nm^2 were applied to the phosphate backbone atoms of the nucleic acid to maintain its initial position. Additionally, similar harmonic positional restraints were applied to each C_a atom of M2-MspA to confine them to their X-ray coordinates [35]. All heavy atoms of the lipid molecules were harmonically constrained to their positions in the structures obtained from the minimization step with a spring constant of 1000 kJ/mol/nm^2 to prevent electroporation. The system was then simulated for 100 ns under the constant number of particles, volume, and temperature (NVT) ensemble with an applied electric field $E = -V/Lz$ along the z-axis to generate a transmembrane potential [36]. The height of the simulation box was set to 22.2 nm. Due to the difficulty of DNA translocation under smaller electric fields, a high electric field of 0.90 V/10 nm was applied for the translocation simulations. Finally, a 100 ns simulation was performed under the NVT ensemble with an applied electric field of 0.045 V/10 nm using the final configuration from the previous simulation as the starting structure. The open pore system was energy minimized for approximately 4500 steps and equilibrated for 10 ns. A subsequent 100 ns simulation was performed under an applied electric field of 0.045 V/10 nm.

To obtain reasonable structures for calculating the ionic current, four initial configurations were designed: the DNA aptamer in the stem-down and loop-down orientations, as well as the Cd^{2+} binding aptamer in the stem-down and loop-down configurations. After energy minimization and equilibrium, these four structures were simulated for 100 ns under an external electric field of 0.90 V/10 nm, with three replicate simulations performed for each configuration. From each set of three, one structure was selected as the initial conformation for calculating the current and further simulated for 100 ns under an electric field of 0.045 V/10 nm, with three replicates for each structure as well. To ensure the accuracy of the calculations, the trajectories from the last 90 ns were extracted to compute the ionic current.

The instantaneous ionic current was calculated using the following equation [37].

$$I(t) = \frac{1}{\Delta t l_z} \sum_{j=1}^{N} q_j \left(z_j(t+\Delta t) - z_j(t)\right)$$

where q_j is the charge of ion j , and $z_j(t+\Delta t) - z_j(t)$ represents the displacement of ion j along the z-axis during the time interval $\Delta t = 0.2$ ns. To minimize the influence of thermal noise, the ionic current was calculated within a 2 nm thick slab centered at the nanopore constriction [38]. All instantaneous currents were accumulated to obtain the

cumulative current.

3. Results

3.1. Design and principle of aptamer-nanopore hybrid sensors

The principle of Cd^{2+} ions sensing in this study is illustrated in Fig. 1. A 25-nucleotide (nt) DNA aptamer (5′-GAC GAC GGG TTC ACA GTC CGT TGTC-3′), previously reported to bind Cd^{2+} with high affinity and specificity, was selected as the recognition element [39,40]. In the absence of Cd^{2+}, this aptamer naturally folds into a stable hairpin structure with a height of 4.34 nm and a width of 1.96 nm (PDB ID: 8GZJ) (Fig. 1a). Upon Cd^{2+} binding (Fig. 1b), coordination through bases G9, C12, and G16 induces conformational rearrangement, reducing the height to 3.56 nm and increasing the width to 2.16 nm [40]. Since both conformations exceed the 1.2 nm constriction of the M2-MspA nanopore (Fig. 1c), we hypothesize that aptamer docking would generate distinct ionic blockades. By analyzing parameters such as the open-pore current (I_0), blocked pore current (I_b), blocking amplitude (ΔI), residual current (I_{res}), blocking ratio ($\Delta I/I_0$), event dwell time (t_{off}), Cd^{2+} can be detected and identified at the single-molecular level.

3.2. Electrical signal characteristics of DNA and DNA_Cd^{2+} in the M2-MspA nanopore

To verify whether the structural changes of the DNA aptamer can be detected by the nanopore, we recorded and analyzed the electrical signal characteristics of DNA and DNA_Cd^{2+} within the nanopore. Since nanopore measurements are typically conducted under high-salt conditions [41,42], the CD spectra of the DNA aptamer upon Cd^{2+} binding were examined in 1 M KCl and 1 M NaCl (Fig. S1). The spectral response of the aptamer-Cd^{2+} complex in 1 M NaCl was comparable to that observed previously under low-ionic-strength buffer conditions [39], and thus 1 M NaCl was selected for subsequent nanopore measurements. In addition, we then analyzed the current-voltage (I–V) characteristics of the bare M2-MspA nanopore and after addition of Cd^{2+}, DNA and DNA_Cd^{2+} (Fig. S2a). The addition of Cd^{2+} alone had little effect on the I–V curve, while DNA and DNA_Cd^{2+} produced distinct current blockade across voltage ranges, with a largest difference observed 100 mV. Therefore, all nanopore experiments were performed at a bias potential of 100 mV.

At this potential, no current events were observed in the presence of Cd^{2+} alone (Fig. S2b), confirming that Cd^{2+} does not generate distinct signals in this system. However, distinct electrical signals were observed for DNA and DNA_Cd^{2+}. Addition of DNA produced consecutive longer-residence, deeper blockades (Fig. 2a), whereas DNA_Cd^{2+} generated shorter-residence, shallower events (Fig. 2b). Event analysis showed that the residual current (I_{res}) of DNA was below 100 pA, whereas that of DNA_Cd^{2+} exceeded 100 pA, indicating two clearly separated populations. Direct comparison of the primary current event types for the two analytes (Fig. 2c and 2d) revealed significant differences in both blocking amplitude (ΔI) and dwell time, enabling clear discrimination between DNA and DNA_Cd^{2+}. Further multidimensional analysis

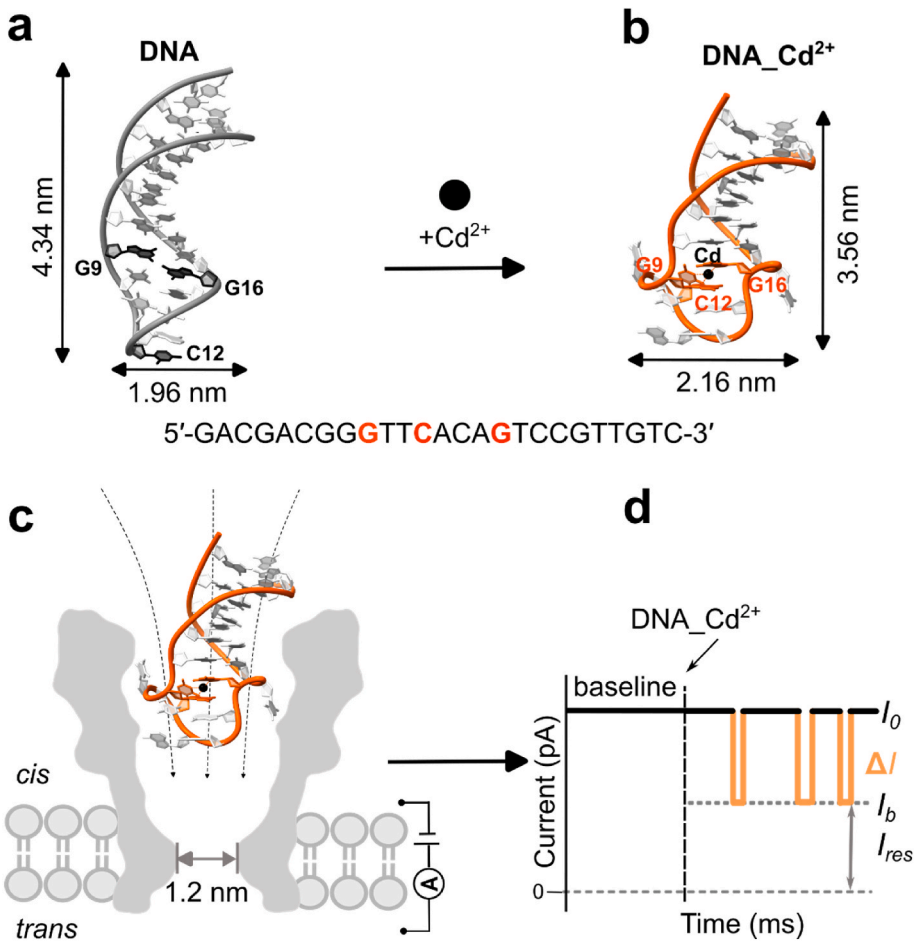

Fig. 1. Principle of Cd^{2+} detection using aptamer-based nanopore sensing method. (a) The native DNA aptamer secondary structure. (b) Structural rearrangement of DNA aptamer after binding with Cd^{2+}. (c) The M2-MspA nanopore for DNA_Cd^{2+} sensing. (d) Schematic representation of the corresponding current changes (ΔI) during DNA docking in the nanopore.

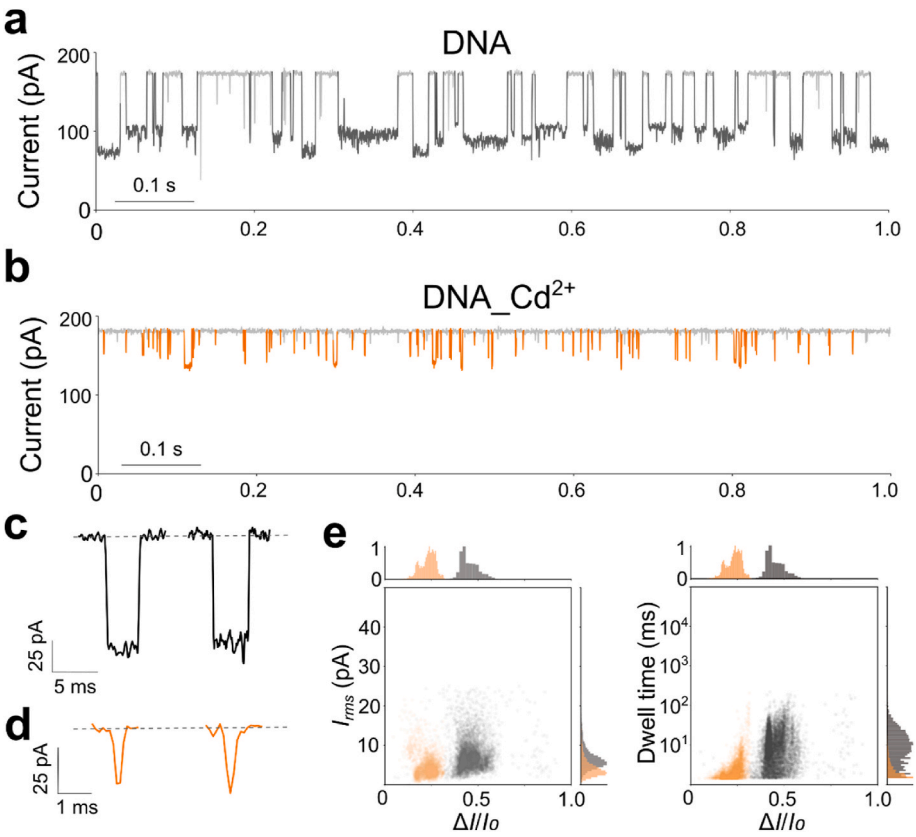

Fig. 2. Electrical characteristics of aptamer and Cd^{2+}-bound aptamer. (a) Representative traces of electrical recordings from a single M2-MspA pore in the presence of DNA (4 μM). (b) Representative traces of electrical recordings from a single pore in the presence of both DNA (4 μM) and Cd^{2+} (5 μM). (c) Typical blocking events for DNA. (d) Typical blocking events for DNA_Cd^{2+}. (e) Scatter plots of current noise (I_{rms}) versus current blockage fraction ($\Delta I/I_0$) for DNA and DNA_Cd^{2+} (left), dwell time versus average current blockage fraction ($\Delta I/I_0$) for DNA and DNA_Cd^{2+} (right). The small histograms above each scatter plot show the distribution of the blockage ratio, with the x-axis representing $\Delta I/I_0$ and the y-axis normalized event counts. All results were derived from the same dataset of DNA and DNA_Cd^{2+}, with DNA at a final concentration of 4 μM and Cd^{2+} at 5 μM. The experiments were carried out at +100 mV in a solution containing 1 M NaCl and 20 mM HEPES (pH 7.3).

combining blockage ratio ($\Delta I/I_0$), root mean square current (I_{rms}) and dwell time demonstrated distinct clustering of events. Specifically, DNA events were predominantly distributed around a $\Delta I/I_0$ of 0.4 (Fig. 2e), whereas DNA_Cd^{2+} events were concentrated near 0.25. This pattern was consistently observed across three independent experiments (Fig. S3a–c), demonstrating the stability and reproducibility of the measurements. These results establish that DNA and DNA_Cd^{2+} can be reliably distinguished in the M2-MspA nanopore, confirming the feasibility of aptamer-based Cd^{2+} detection.

3.3. Molecular dynamics of DNA and DNA_Cd^{2+} in M2-MspA nanopores

To elucidate the mechanisms underlying the distinct blockade amplitudes and kinetics observed experimentally, we performed all-atom molecular dynamics (MD) simulations and three replicate simulations were performed for each condition. Representative simulation trajectories for both loop-down and stem-down conformations are provided in Supplementary Movies S1–S12. As shown in Fig. 3a and b, native DNA was able to penetrate deeply into the M2-MspA nanopore, reaching a maximum depth of ~5 nm within 100 ns, regardless of whether it entered in the loop-down or stem-down orientation. In contrast, the DNA_Cd^{2+} only reached ~1.5 nm and remained largely confined to the pore entrance, reflecting its larger conformational width compared with unbound DNA.

To further investigate the effects of conformation and charge differences on the ionic current, we calculated the ionic current under a field of 0.045 V/10 nm (+100 mV) once the molecules reached their deepest penetration point. As shown in Fig. 3c, DNA produced a steeper cumulative current slope, corresponding to a higher instantaneous current and stronger ion flow obstruction, whereas DNA_Cd^{2+} displayed a much shallower slope, consistent with weaker blockade signals. By linearly fitting the slope of the cumulative current curves, we extracted the instantaneous ionic currents and converted them into corresponding blockade ratios (Fig. 3d). Comparison with experimental data (dashed lines in Fig. 3d) revealed that the loop-down orientation yielded simulation results (DNA: 42 %, DNA_Cd^{2+}: 22 %) closest to the experimental measurements (DNA: 43 %, DNA_Cd^{2+}: 25 %). Entry orientation analysis further indicated that both native DNA and the DNA_Cd^{2+} preferentially adopted the loop-down orientation, with approximately 60 % of events occurring in this mode. Although molecular dynamics (MD) simulations did not reveal a statistically significant bias between loop-down and stem-down orientation, repeated nanopore experiments consistently confirmed that the loop-down orientation is the preferred entry mode for both analytes. Together, these findings demonstrate that Cd^{2+} binding restricts aptamer penetration, reduces ionic blockade, and that loop-down entry is the preferred orientation for both DNA and DNA_Cd^{2+}.

3.4. Selectivity performance of aptamer conformation sensing in complex matrices

Confident in the Cd^{2+} detection capabilities based on the conformational capabilities of aptamers within a nanopore, we further evaluated the selectivity of this strategy. Six common metal ions (Mn^{2+}, Ca^{2+}, Cu^{2+}, Co^{2+}, Ni^{2+}, and Fe^{3+}) with chemical properties similar to Cd^{2+} and frequently coexisting in natural water sources were selected as

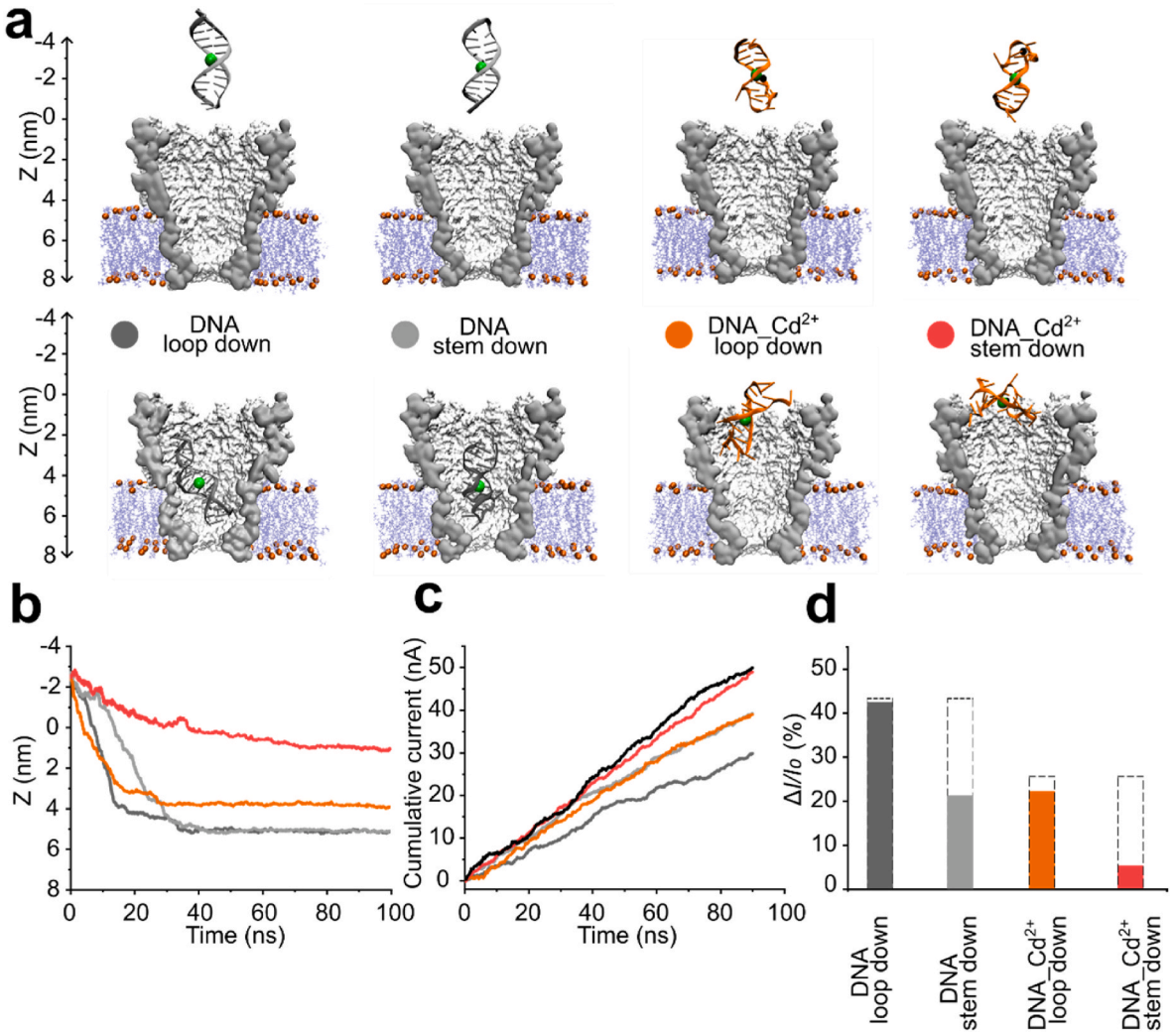

Fig. 3. MD analysis of DNA and DNA_Cd^{2+} entry into a nanopore. (a) Original and equilibrated structures of DNA and DNA_Cd^{2+} entering an M2-MspA nanopore. These conformations are referred to as stem-down and loop-down. The green sphere on each conformation indicates the center of mass. (b) Z-coordinates of the center of mass for DNA and DNA_Cd^{2+} as a function of time for simulations with loop-down or stem-down conformations. (c) Simulated cumulative ion currents through the pore for different states: open pore (black), DNA loop-down (Dark grey), DNA stem-down (light grey), DNA_Cd^{2+} loop-down (orange), and DNA_Cd^{2+} stem-down (red). An external electric field of 0.045 V/10 nm was applied, corresponding to a voltage bias of +100 mV. (d) Derived ionic currents for different sensing states have been converted into blockage ratios for clearer presentation. The dotted boxes represent the results of the nanopore experiment. All experiments were performed in triplicate. (For interpretation of the references to color in this figure legend, the reader is referred to the Web version of this article.)

potential interfering species. The DNA aptamer exhibited characteristic current signals and distinct event features only in the presence of Cd^{2+}; no such responses were observed with the other metal ions (Fig. S4 and S5). Analysis of current blockage ratios indicated that mixtures of DNA with Mn^{2+}, Ca^{2+}, Cu^{2+}, Co^{2+}, Ni^{2+}, and Fe^{3+} produced ratios closely aligned with that of DNA alone, which was ~42 % (Fig. 4a). In contrast, Cd^{2+} produced a distinctly different and highly distinguishable blockage ratio of ~22 %. Noise analysis further supported this distinction (Fig. 4b). Cu^{2+} and Cd^{2+} both induced low-noise events with peak levels below 5 pA, whereas other metal ions generated moderate noise levels of 5–10 pA, DNA alone exhibited the highest noise, with peaks exceeding 10 pA. These results indicate that although other ions may weakly interact with the aptamer, only Cd^{2+} binding produces a uniquely identifiable signal. It is worth noting that DNA and DNA_Cd^{2+} events exhibited substantial overlap in their dwell time distributions (Fig. S6).

To enhance discrimination, pore-blockage ratios and I_{rms} were analyzed simultaneously (Fig. 4c). Only DNA_Cd^{2+} exhibited events with $\Delta I/I_0 < 25$ % and $I_{rms} < 5$ pA, while DNA and DNA_metal complexes cluster together. To balance sensitivity and specificity, we employed two complementary strategies: (i) a direct method quantifying the increase of DNA_metal complex events ($\Delta I/I_0 = 12.5$–30 %), and (ii) an indirect method measuring the reduction of DNA events ($\Delta I/I_0 = 30$–55 %). Together, these approaches delineate the ion-specific binding behavior of DNA. Detailed calculation procedures are provided in the Methods section. Both analyses demonstrated superior selectivity for Cd^{2+}, with specificity values of ~93 %, whereas all other ions yielded values below 5 % (Fig. 4d).

Finally, validation in a mixed-ion system containing Cd^{2+} and all six other metals confirmed that the aptamer retained its strong binding preference for Cd^{2+}. Event clusters for Cd^{2+} remained clearly separated from those of other ions and DNA alone (Fig. S7), demonstrating that the aptamer–nanopore system enables reliable Cd^{2+} detection even in the presence of multiple competing ions.

3.5. *Quantitative detection mode of aptamer conformation sensing*

Building on the high selectivity of our approach in Cd^{2+} detection, we next evaluated the sensitivity and establish a standard curve for quantitative analysis. To exclude potential effects of DNA concentration on event recognition, we first investigated the relationship between

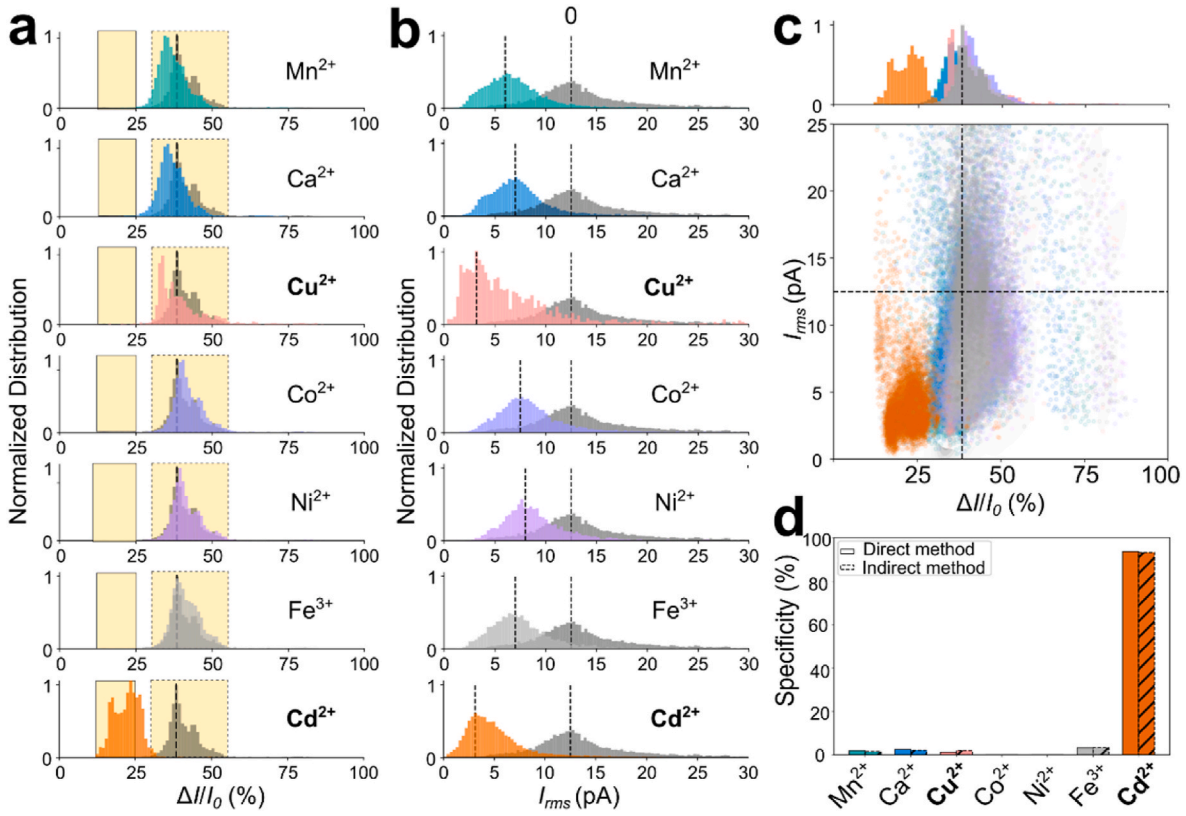

Fig. 4. Selectivity of the Cd^{2+} nanopore sensor. (a) Relative current change ($\Delta I/I_0$) for different metal ions. The x-axis represents the block ratio ($\Delta I/I_0$=(I_0 - I_b)/I_0), and the y-axis shows normalized event frequency. The shaded area represents DNA alone, with the dashed line marking its peak. The solid black box highlights DNA_Cd^{2+} events ($\Delta I/I_0$ = 12.5–30 %), and the dashed box indicates DNA events ($\Delta I/I_0$ = 30–55 %). (b) Current noise (I_{rms}) for different metal ions. The x-axis shows blockade ratio noise (I_{rms}), and the y-axis represents normalized event frequency. The shaded region shows DNA alone, with the dashed line marking its peak. (c) Correlation between current noise and mean blockage current. The top histogram shows event frequency vs. $\Delta I/I_0$ (%), and the scatter plot below shows I_{rms} vs $\Delta I/I_0$ (%). Colors indicate different metal ions and black dashed lines mark the peak values for DNA events. (d) Evaluation of DNA specificity with different metal ions was performed using both direct (x = 12.5–30 %) and indirect (x = 30–55 %) methods, with detailed results from the direct calculation method presented (see Experimental section). Nanopore measurements were recorded at +100 mV in 1 M NaCl and 20 mM HEPES (pH 7.3), with 4 μM aptamer and 5 μM metal ions in the cis solution. (For interpretation of the references to color in this figure legend, the reader is referred to the Web version of this article.)

DNA concentration and event frequency. The result showed a linear increase in event frequency up to 2 μM DNA, while saturation was observed above 6 μM (Fig. S8a, Fig. 5a). Therefore, a 4 μM DNA concentration was selected to investigate the changes in DNA_Cd^{2+} and DNA events across varying Cd^{2+} concentrations.

With increasing Cd^{2+} concentration, the proportion of DNA_Cd^{2+} events increased progressively, accompanied by a corresponding decrease in DNA events (Fig. S8b). Based on these observations, two calibration strategies were developed: Method 1 tracked the increase in DNA_Cd^{2+} events, whereas Method 2 monitored the decrease in DNA events (Fig. 5b and c). Method 1 produced a linear range from 312.50 nM to 5.00 μM with a limit of detection (LOD) of 33.80 nM (LOD = 3 × standard deviation above the mean of blank samples), whereas Method 2 yielded a linear range from 156.25 nM to 5.00 μM with a higher LOD of 90.90 nM. These results demonstrate that Cd^{2+} ions can be quantitatively detected by monitoring shifts in the relative proportions of DNA

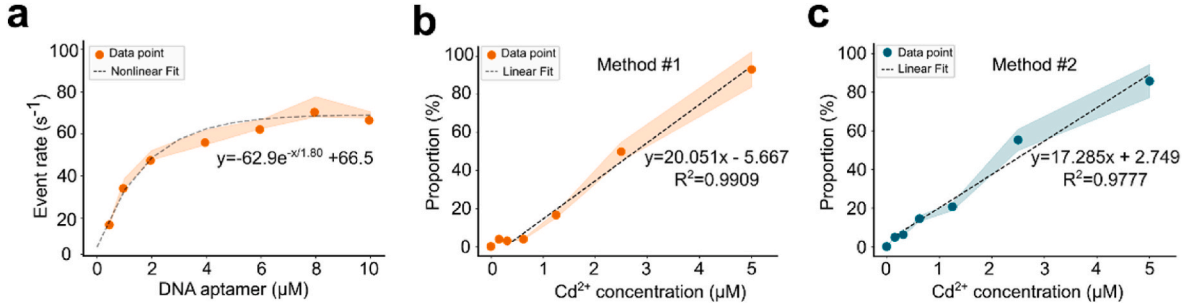

Fig. 5. Sensitivity of the Cd^{2+} nanopore sensor. (a) The plot of event frequency versus DNA concentration. The x-axis represents the concentration of added DNA, and the y-axis indicates the frequency of current events. The dashed line represents the nonlinear fit. (b) Dose-response curve 1 (method #1). The x-axis represents a mixture of 4 μM DNA and varying concentrations of Cd^{2+}, while the y-axis shows the increase in the number of DNA_Cd^{2+} complex events. (c) Dose-response curve 2 (method #2). The x-axis represents a mixture of 4 μM DNA and varying concentrations of Cd^{2+}, while the y-axis shows the decrease in the number of free DNA events. Specific calculation methods can be found in the Experimental section. The dashed line represents the linear fit. Nanopore measurements were recorded at +100 mV in 1 M NaCl and 20 mM HEPES (pH 7.3). Each experiment was conducted in triplicate.

and DNA_Cd^{2+} events, providing a cross-validation approach for practical applications.

3.6. Application of aptamer conformation sensing strategy in various water samples

Encouraged by the high selectivity and sensitivity of our nanopore system for Cd^{2+} detection, we investigated its suitability in real-world water samples, including tap water, river water (Dasha River), and seawater (Qianhai Bay). Samples were filtered through a 0.22 μm membrane and spiked with 5.00 μM Cd^{2+} for recovery analysis (Fig. 6a). Results obtained using ICP-MS and the nanopore sensor were compared. To exclude interference from random nucleic acids, untreated water samples were directly introduced into the nanopore (Fig. S9), yielding no significant signals, consistent with the reported ultralow nucleic acid levels in natural waters [43,44].

For tap water, ICP-MS reported a recovery rate of 96.44 ± 0.34 % while the nanopore sensor gave nearly identical values (Method 1: 92.77 ± 1.30 %; Method 2: 95.13 ± 1.47 %). Similarly, in river water, ICP-MS yielded 96.52 ± 0.56 %, and the nanopore sensor achieved 100.31 ± 0.97 % (Method 1) (Table 1) and 100.28 ± 3.33 % (Method 2). These findings indicate that matrix components in tap and river water do not significantly interfere with Cd^{2+} detection.

In contrast, untreated seawater samples showed poor recovery with the nanopore sensor (Method 1: 22.59 ± 2.44 % and Method 2: 32.72 ± 10.45 %), likely due to the interference from organic compounds [45,46]. After pretreatment with dilute nitric acid, recovery rates improved significantly, reaching 79.24 ± 3.21 % for Method 1 and 87.74 ± 2.88 % for Method 2 (Fig. 6b and c), mainly because acid oxidation disrupted metal-organic complexes and dissolved carbonate and hydroxide species, releasing free Cd^{2+} [47]. For comparison, the ICP method achieved a recovery rate of 85.88 ± 0.68 % (Table 1). Overall, these findings demonstrate that the nanopore aptamer sensor provides accurate Cd^{2+} quantification in tap and river water without pretreatment and, with simple nitric acid pretreatment, is also suitable for seawater.

Table 1
Recovery rate of Cd^{2+} Ions from different types of water samples.

Method	Sample type	T-value (μM)	E-value (μM)	Recovery rate (%)
ICP-MS	Tap water	5.00	4.82 ± 0.02	96.44 ± 0.34
	River water	5.00	4.83 ± 0.03	96.52 ± 0.56
	Seawater	5.00	4.30 ± 0.03	85.88 ± 0.68
method 1	Tap water	5.00	4.64 ± 0.07	92.77 ± 1.30
	River water	5.00	5.02 ± 0.05	100.31 ± 0.97
	Seawater	5.00	1.13 ± 0.12	22.59 ± 2.44
	Pretreated Seawater	5.00	3.96 ± 0.16	79.24 ± 3.21
method 2	Tap water	5.00	4.76 ± 0.07	95.13 ± 1.47
	River water	5.00	5.01 ± 0.17	100.28 ± 3.33
	Seawater	5.00	1.64 ± 0.52	32.72 ± 10.45
	Pretreated Seawater	5.00	4.39 ± 0.14	87.74 ± 2.88

* T-value denotes the theoretical value, while E-value refers to the values obtained from our experiments. Recovery rate = E-value/T-value*100 %.
*Each experimental value represents the mean of three replicate analyses ± one standard deviation.

4. Discussion

This study demonstrates that the conformation sensing of specific

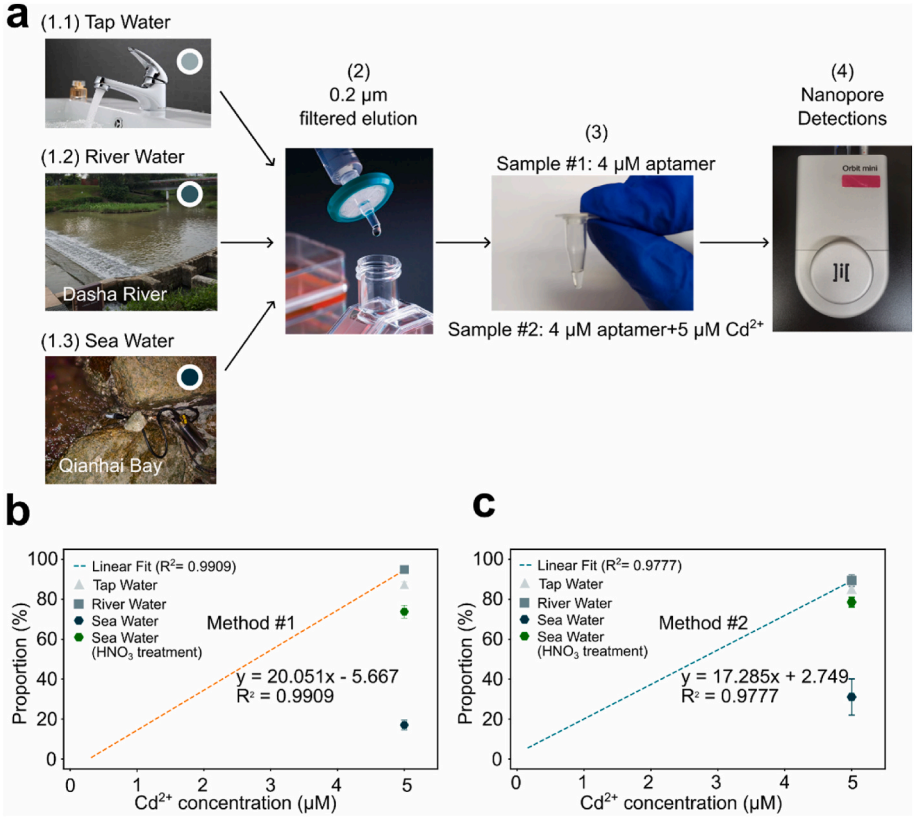

Fig. 6. Performance of detection in different types of water samples. (a) Schematic diagram of the detection process. Different colors represent different water samples. (b) Data from the detection of Cd^{2+} in different water samples were plotted using dose-response curve 1. (c) Data from the detection of Cd^{2+} in different water samples were plotted using dose-response curve 2. Nanopore measurements were recorded at +100 mV in 1 M NaCl and 20 mM HEPES (pH 7.3), with 4 μM aptamer and 5 μM metal ions in the cis solution. Each experiment was conducted in triplicate. (For interpretation of the references to color in this figure legend, the reader is referred to the Web version of this article.)

DNA within the M2-MspA nanopore provides an effective strategy for quantitative detection of Cd^{2+} [48,49]. Optimal discrimination between Cd^{2+}-bound aptamers and unbound aptamers was achieved in 1 M NaCl at an +100 mV, ensuring both high binding efficiency and signal stability. In the absence of Cd^{2+}, the aptamer produced long-lived, deep current blockades, whereas Cd^{2+} binding led to shorter, shallower events, indicating distinct conformational and electrophoretic changes. Molecular dynamics simulations confirmed that Cd^{2+} coordination induces specific structural rearrangements that alter aptamer-nanopore interactions and modulate the ionic current.

The nanopore-integrated aptamer enabled highly sensitive and selective Cd^{2+} detection. Distinct blockade signatures were clearly distinguishable from those of other metal ions, and although minor Cu^{2+} interference was observed, Cd^{2+} specificity remained dominant. Quantitative analysis further showed a linear response between 312.50 nM and 5.00 μM, with a limit of detection (LOD) of 33.80 nM, which meets the surface water quality standard for Cd^{2+} (10 μg/L, ~88.9 nM; Ministry of Ecology and Environment, 2002) [50]. Compared with conventional aptamer-based Cd^{2+} assays such as electrochemical [51], colorimetry [52], enzymatic [53], and fluorescent methods [54], this nanopore approach eliminates the need for enzymes or dyes and enables direct , enzyme-free, single-molecule detection.

The method was further validated in real water samples, including tap water, river water, and seawater. Near 100 % recoveries were obtained for tap and river water, consistent with ICP-MS results, confirming negligible matrix interference. In seawater, reduced recovery was attributed to organic matter; however, pretreatment with dilute nitric acid significantly restored detection accuracy, achieving recoveries of 79.24–87.74 %. The reduced recovery in seawater can be attributed to organic and complexing substances that interfere with Cd^{2+}-aptamer binding [55–57], while the improved recovery after HNO_3 pretreatment confirms that acid treatment effectively eliminates these interferences by releasing free Cd^{2+} [58,59]. These findings further demonstrate the method's robustness and potential applicability to a wide range of environmental water samples.

In summary, the proposed nanopore-based aptamer sensor offers a simple, sensitive, and selective strategy for Cd^{2+} detection in complex aqueous environments. Future work will focus on refining signal recognition algorithms and investigating the effects of higher salt concentrations, pH, and temperature to further enhance sensing performance and broaden applicability to other toxic metal ions.

CRediT authorship contribution statement

Shujun He: Validation, Investigation, Data curation. **Ronghui Liu:** Writing – review & editing, Writing – original draft, Supervision, Investigation, Data curation. **Xinxin Bao:** Software, Formal analysis, Data curation. **Jiayuan Pang:** Validation, Formal analysis. **Xi Zhang:** Validation, Formal analysis. **Yue Liu:** Validation. **Wenfu Lin:** Validation. **Jiadun Liu:** Validation. **Tianxin Li:** Validation. **Yao Li:** Writing – review & editing, Software, Project administration. **Yi Li:** Writing – review & editing, Supervision, Project administration, Methodology, Funding acquisition, Data curation. **Xinrong Guo:** Writing – review & editing, Supervision, Project administration, Methodology, Funding acquisition, Data curation.

Declaration of competing interest

The authors declare that they have no known competing financial interests or personal relationships that could have appeared to influence the work reported in this paper.

Acknowledgments

Ronghui Liu acknowledges support from the Science and Technology Innovation Commission of Shenzhen (JCYJ20230807092459028) and the National Natural Science Foundation of China (32371526, 32100021). Xinrong Guo acknowledges support from the National Natural Science Foundation of China (82404318), the Guangdong Basic and Applied Basic Research Foundation (2022A1515140191), the Guangdong Medical Science and Technology Research Fund Project (A2024159), the Youth Research Projects of Guangdong Medical University (GDMUD2024010), and the Funds for PhD Researchers of Guangdong Medical University (GDMUB2021004). Yi Li acknowledges support from the National Natural Science Foundation of China (62171211) and the Science and Technology Innovation Commission of Shenzhen (JCYJ20220814170440001, JCYJ20220818100218039, JCYJ20220530113013030). Yao Li acknowledges support from the National Natural Science Foundation of China (12275137).

Appendix A. Supplementary data

Supplementary data to this article can be found online at https://doi.org/10.1016/j.aca.2025.344964.

Data availability

No data was used for the research described in the article.

References

[1] B. Heidt, W.F. Siqueira, K. Eersels, H. Diliën, B. van Grinsven, R.T. Fujiwara, T. J. Cleij, Point of care diagnostics in resource-limited settings: a review of the present and future of PoC in its Most needed environment, Biosensors (Basel) 10 (10) (2020) 133.
[2] M. Li, Q. Shi, N. Song, Y. Xiao, L. Wang, Z. Chen, T.D. James, Current trends in the detection and removal of heavy metal ions using functional materials, Chem. Soc. Rev. 52 (17) (2023) 5827–5860.
[3] F. Chen, C. Zhi, A.F. Yousef, H.M. Rizwan, M.M. Ali, Analysis of toxic elements in leaves and fruits of loquat by inductively coupled plasma-mass spectrometry (ICP-MS), Acta Scientiarum Polonorum Hortorum Cultus 20 (5) (2021) 33–42.
[4] A. Sussulini, R.A. Hauser-Davis, Metallomics applied to the Study of neurodegenerative and mental diseases, Adv. Exp. Med. Biol. 1055 (2018) 21–37.
[5] M.R. Awual, M. Khraisheh, N.H. Alharthi, M. Luqman, A. Islam, M. Rezaul Karim, M.M. Rahman, M.A. Khaleque, Efficient detection and adsorption of cadmium(II) ions using innovative nano-composite materials, Chem. Eng. J. 343 (2018) 118–127.
[6] S.K. Rai, R. Xalxo, T.K. Patle, A. Verma, R. Chauhan, P.K. Mahish, Analyzing Contamination of Heavy Metals - AAS and Fluorescence Spectroscopy//Heavy metals in the environment: management strategies for global pollution, Am. Chem. Soc. (2023) 167–204.
[7] O. Mestek, M. Loula, A. Kaňa, M. Vosmanská, Can ultrafast single-particle analysis using ICP-MS affect the detection limit? Case study: silver nanoparticles, Talanta 210 (2020) 120665.
[8] L. Wang, H. Wang, X. Chen, S. Zhou, Y. Wang, X. Guan, Chemistry solutions to facilitate nanopore detection and analysis, Biosens. Bioelectron. 213 (2022) 114448.
[9] Y. Wang, Y. Zhao, A. Bollas, Y. Wang, K.F. Au, Nanopore sequencing technology, bioinformatics and applications, Nat. Biotechnol. 39 (11) (2021) 1348–1365.
[10] B. Lin, J. Hui, H. Mao, Nanopore technology and its applications in gene sequencing, Biosensors (Basel) 11 (7) (2021) 214.
[11] L.Q. Gu, J.W. Shim, Single molecule sensing by nanopores and nanopore devices, Analyst 135 (3) (2010) 441–451.
[12] Y. Zhang, C. Hu, R. Liu, S. He, J. Yang, W. Yao, Y. Li, X. Guo, Protein nanopore-based sensors for public health analyte detection, J. Mater. Chem. B 12 (39) (2024) 9845–9862.
[13] L. Liu, C. Zhang, W. Jiang, X. Li, Y. Dai, H. Jia, Understanding the sorption behaviors of heavy metal ions in the interlayer and nanopore of montmorillonite: a molecular dynamics study, J. Hazard Mater. 416 (2021) 125976.
[14] P. Arora, H. Zheng, S. Munusamy, R. Jahani, L. Wang, X. Guan, Probe-assisted detection of Fe(3+) ions in a multi-functionalized nanopore, Biosens. Bioelectron. 251 (2024) 116125.
[15] J. Kasianowicz, B. Walker, K. Musti, H. Bayley, Genetically engineered pores as metal ion biosensors, MRS Proceedings 330 (2011) 217.
[16] S. Wang, J. Cao, W. Jia, W. Guo, S. Yan, Y. Wang, P. Zhang, H.Y. Chen, S. Huang, Single molecule observation of hard-soft-acid-base (HSAB) interaction in engineered Mycobacterium smegmatis porin A (MspA) nanopores, Chem. Sci. 11 (3) (2019) 879–887.
[17] W. Sun, Y. Xiao, K. Wang, S. Zhang, L. Yao, T. Li, B. Cheng, P. Zhang, S. Huang, Nanopore discrimination of rare earth elements, Nat. Nanotechnol. 20 (4) (2025) 523–531.
[18] J. Byun, Recent progress and opportunities for nucleic acid aptamers, Life 11 (3) (2021) 193.

[19] J.M. Seibold, S.W. Abeykoon, A.E. Ross, R.J. White, Development of an electrochemical, aptamer-based sensor for dynamic detection of neuropeptide Y, ACS Sens. 8 (12) (2023) 4504–4511.
[20] W. Guo, C. Hu, S. Li, D. Wei, J. Zhou, X. Liu, H. Chen, S. Li, Y. Deng, Selection and electrochemical-sensor application of an DNA-aptamer for methyl parathion detection, Anal. Chim. Acta 1241 (2023) 340780.
[21] H. Yu, O. Alkhamis, J. Canoura, Y. Liu, Y. Xiao, Advances and challenges in small-molecule DNA aptamer isolation, characterization, and sensor development, Angew Chem. Int. Ed. Engl. 60 (31) (2021) 16800–16823.
[22] H. Zhou, Y. Li, W. Wu, Aptamers: promising reagents in biomedicine application, Adv Biol (Weinh) 8 (6) (2024) 2300584.
[23] A.S. Shraim, B.A. Abdel Majeed, M.A. Al-Binni, A. Hunaiti, Therapeutic potential of aptamer-protein interactions, ACS Pharmacol. Transl. Sci. 5 (12) (2022) 1211–1227.
[24] J. Zhou, Y. Sun, J. Zhang, F. Luo, H. Ma, M. Guan, J. Feng, X. Dong, Dumbbell aptamer sensor based on dual biomarkers for early detection of Alzheimer's Disease, ACS Appl. Mater. Interfaces 15 (13) (2023) 16394–16407.
[25] Z. Su, Y. Kong, T. Li, Y. Zhao, X. Zhang, D. Wu, Y. Wu, G. Li, An aptamer-triggered hybridization chain reaction strategy for ultra-sensitive biological nanopore detection of aflatoxin B1, Sensor. Actuator. B Chem. 407 (2024) 135457.
[26] R. Mo, L. He, X. Yan, T. Su, C. Zhou, Z. Wang, P. Hong, S. Sun, C. Li, A novel aflatoxin B1 biosensor based on a porous anodized alumina membrane modified with graphene oxide and an aflatoxin B1 aptamer, Electrochem. Commun. 95 (2018) 9–13.
[27] Jiadun Liu, Luoan Xiong, Yuhang Hu, Zhuofei Wang, Jing Dai, Tie Li, Xinrong Guo, Ronghui Liu, Zhongbo Yu, Yao Li, Yi Li, Probing structural variants of irregular DNA G-tracts ($n \leq 2$) using MspA nanopores, ACS Appl. Mater. Interfaces 17 (9) (2025) 13415–13426.
[28] M.J. Abraham, T. Murtola, R. Schulz, S. Páll, J.C. Smith, B. Hess, E. Lindahl, GROMACS: high performance molecular simulations through multi-level parallelism from laptops to supercomputers, SoftwareX 1–2 (2015) 19–25.
[29] S. Jo, T. Kim, V.G. Iyer, W. Im, CHARMM-GUI: a web-based graphical user interface for CHARMM, J. Comput. Chem. 29 (11) (2008) 1859–1865.
[30] W. Jorgensen, J. Chandrasekhar, J. Madura, R. Impey, M. Klein, Comparison of simple potential functions for simulating liquid water, J. Chem. Phys. 79 (1983) 926–935.
[31] G. Bussi, D. Donadio, M. Parrinello, Canonical sampling through velocity rescaling, J. Chem. Phys. 126 (1) (2007).
[32] M. Bernetti, G. Bussi, Pressure control using stochastic cell rescaling, J. Chem. Phys. 153 (11) (2020) 114107.
[33] B. Hess, H. Bekker, H.J.C. Berendsen, J.G.E.M. Fraaije, LINCS: a linear constraint solver for molecular simulations, J. Comput. Chem. 18 (12) (1997) 1463–1472.
[34] S. Miyamoto, P.A. Kollman, Settle: an analytical version of the SHAKE and RATTLE algorithm for rigid water models, J. Comput. Chem. 13 (8) (1992) 952–962.
[35] A.T. Brünger, Free R value: a novel statistical quantity for assessing the accuracy of crystal structures, Nature 355 (6359) (1992) 472–475.
[36] J. Gumbart, F. Khalili-Araghi, M. Sotomayor, B. Roux, Constant electric field simulations of the membrane potential illustrated with simple systems, Biochim. Biophys. Acta 1818 (2) (2012) 294–302.
[37] A. Aksimentiev, J.B. Heng, G. Timp, K. Schulten, Microscopic kinetics of DNA translocation through synthetic nanopores, Biophys. J. 87 (3) (2004) 2086–2097.
[38] H. Brinkerhoff, A.S.W. Kang, J. Liu, A. Aksimentiev, C. Dekker, Multiple rereads of single proteins at single-amino acid resolution using nanopores, Science 374 (6574) (2021) 1509–1513.
[39] H. Wang, H. Cheng, J. Wang, L. Xu, H. Chen, R. Pei, Selection and characterization of DNA aptamers for the development of light-up biosensor to detect Cd(II), Talanta 154 (2016) 498–503.
[40] H. Liu, Y. Gao, J. Mathivanan, Z. Armour-Garb, Z. Shao, Y. Zhang, X. Zhao, Q. Shao, W. Zhang, J. Yang, C. Cao, H. Li, J. Sheng, J. Gan, Crystal structures and identification of novel Cd^{2+}-specific DNA aptamer, Nucleic Acids Res. 51 (9) (2023) 4625–4636.
[41] P.M. Vlahovska, R.S. Gracià, S. Aranda-Espinoza, R. Dimova, Electrohydrodynamic model of vesicle deformation in alternating electric fields, Biophys. J. 96 (12) (2009) 4789–4803.
[42] R.C.A. Versloot, F.L.R. Lucas, L. Yakovlieva, M.J. Tadema, Y. Zhang, T.M. Wood, N. I. Martin, S.J. Marrink, M.T.C. Walvoort, G. Maglia, Quantification of protein glycosylation using nanopores, Nano Lett. 22 (13) (2022) 5357–5364.
[43] B. Zhao, P.M. van Bodegom, K.B. Trimbos, Bacterial abundance and pH associate with eDNA degradation in water from various aquatic ecosystems in a laboratory setting, Front. Environ. Sci. 11 (2023) (2023) 1025105.
[44] C.R. Turner, K.L. Uy, R.C. Everhart, Fish environmental DNA is more concentrated in aquatic sediments than surface water, Biol. Conserv. 183 (2015) 93–102.
[45] M. Plavšić, S. Karavoltsos, J. Schijf, Editorial: Metal-organic interactions in seawater under changing anthropogenic and climate conditions, Front. Mar. Sci. 10 (2023) 1215306, 2023.
[46] R. Yang, C.M.G. van den Berg, Metal complexation by humic substances in seawater, Environmental Science & Technology 43 (19) (2009) 7192–7197.
[47] M. Kilic, S. Kilic, S. Yenisoy-Karakaş, The method development for elimination of matrix interferences in seawater monitoring to determine elements by ICP-MS, Environ. Monit. Assess. 195 (1) (2022) 180.
[48] I. Heaton, M. Platt, Multiuse Nanopore platform with disposable paper analytical device for the detection of heavy metal ions, Ind. Eng. Chem. Res. 59 (49) (2020) 21403–21412.
[49] C.H. Zhang, G.J. Li, J.H. Wang, Application of Nanopore and Porous Materials for Heavy Metal Ion Detection, Fenxi Huaxue/Chinese Journal of Analytical Chemistry, 2014.
[50] C. Ministry of Ecology and Environment, Surface Water Environmental Quality Standard, GB 3838-2002, 2002.
[51] H.R. Lotfi Zadeh Zhad, Y.M. Rodríguez Torres, R.Y. Lai, A reagentless and reusable electrochemical aptamer-based sensor for rapid detection of Cd(II), J. Electroanal. Chem. 803 (2017) 89–94.
[52] D. Zhou, W. Wu, Q. Li, J. Pan, J. Chen, A label-free and enzyme-free aptasensor for visual Cd^{2+} detection based on split DNAzyme fragments, Anal. Methods 11 (28) (2019) 3546–3551.
[53] L. Zeng, J. Gong, P. Rong, C. Liu, J. Chen, A portable and quantitative biosensor for cadmium detection using glucometer as the point-of-use device, Talanta 198 (2019) 412–416.
[54] B. Zhou, X.-Y. Yang, Y.-S. Wang, J.-C. Yi, Z. Zeng, H. Zhang, Y.-T. Chen, X.-J. Hu, Q.-L. Suo, Label-free fluorescent aptasensor of Cd^{2+} detection based on the conformational switching of aptamer probe and SYBR green I, Microchem. J. 144 (2019) 377–382.
[55] X. Tu, P. Xu, Y. Zhu, W. Mi, Y. Bi, Molecular complexation properties of Cd^{2+} by algal organic matter from Scenedesmus obliquus, Ecotoxicol. Environ. Saf. 263 (2023) 115378.
[56] R. Ma, Y. Feng, H. Li, M. Liu, Y. Cui, J. Wang, K. Shen, S. Zhang, S. Tong, Deep-sea microorganisms-driven V5+ and Cd^{2+} removal from vanadium smelting wastewater: bacterial screening, performance and mechanism, Environmental Pollution 360 (2024) 124599.
[57] H. Cui, C. Zhang, C. Song, L. Xie, G. Zhang, L. Zhao, Y. Zhao, Z. Wei, Remediation of solid wastes and stabilization of heavy metal contaminations using Humid Acid ligands, ACS Sustainable Resource Management 1 (3) (2024) 471–479.
[58] D. Gondar, R. López, S. Fiol, J.M. Antelo, F. Arce, Cadmium, lead, and copper binding to humic acid and fulvic acid extracted from an ombrotrophic peat bog, Geoderma 135 (2006) 196–203.
[59] R.A. Saar, J.H. Weber, Complexation of cadmium(II) with water- and soil-derived fulvic acids: effect of pH and fulvic acid concentration, Can. J. Chem. 57 (11) (1979) 1263–1268.